Dynamics of Reversed Urban Breeze Circulation

Jaemyeong Mango Seo

School of Earth and Environmental Sciences, Seoul National University, Seoul, South Korea

Gantuya Ganbat

School of Earth and Environmental Sciences, Seoul National University, Seoul, South Korea, and Information and Research Institute of Meteorology, Hydrology, and Environment, Ulaanbaatar, Mongolia

Jong-Jin Baik

School of Earth and Environmental Sciences, Seoul National University, Seoul, South Korea

(Manuscript received 27 September 2016, in final form 16 December 2016)

ABSTRACT

The urban breeze circulation (UBC) is a thermally forced mesoscale circulation that is characterized by low-level inward flow toward the urban center, updrafts near the urban center, upper-level outward flows, and weak downdrafts outside the urban area. Previous numerical modeling studies indicate that in the early morning the direction of the UBC can be reversed. Here, the dynamics of a reversed UBC is studied in the context of the response of the atmosphere to specified thermal forcing, which represents diurnally varying urban heating. For this, a linearized, two-dimensional, hydrostatic, Boussinesq airflow system in a rotating frame with specified thermal forcing is solved using the Fourier transform method. The occurrence of a reversed UBC in the early morning is confirmed. The Coriolis parameter affects the strength and vertical structure of the UBC, whose role is similar to that of the coefficient of Rayleigh friction and Newtonian cooling. The occurrence condition, strength, and vertical structure of a reversed UBC are examined. The Coriolis force as well as urban heating alters the occurrence time of the reversed UBC. For a strongly viscous system, a reversed UBC occurs only in high latitudes with low occurrence possibility. A simple oscillation-type model for the horizontal velocity is constructed to get some dynamical insights into a reversed UBC. The analysis results also show that the Coriolis force alters the occurrence time of the reversed UBC.

1. Introduction

Weather and climate in urban areas are influenced by the local circulation induced by a thermal difference between urban and rural areas, which is called the urban breeze circulation (UBC) or the urban heat island circulation. A UBC can interact with other local circulations such as sea–land breeze circulation and mountain–valley breeze circulation, depending on the geographical location (Dandou et al. 2009; Ryu and Baik 2013). The UBC is one of the interesting problems in mesoscale meteorology, and a better understanding of UBCs will help urban planning as well as urban weather and air quality prediction (Barlag and Kuttler 1990; Ryu et al. 2013b).

The UBC has been extensively studied in the past. Observational studies have documented UBC and its features (Clarke 1969; Oke 1973; Shreffler 1978, 1979; Haeger-Eugensson and Holmer 1999; Lindén and Holmer 2011). Numerical modeling studies have illustrated the structure and evolution of simulated UBCs (Draxler 1986; Lemonsu and Masson 2002; Ryu et al. 2013b). Theoretical studies have examined urban heating–induced circulation/flow by adding surface temperature perturbations in a mechanically viscous and thermally diffusive system (Estoque and Bhumralkar 1969; Olfe and Lee 1971) or thermal forcing in the thermodynamic energy equation (Lin and Smith 1986; Baik 1992; Han and Baik 2008).

To investigate a diurnal cycle of the UBC in a theoretical frame, the observed diurnal variation of urban heating has to be considered. Observational studies indicate that the urban heat island intensity exhibits a diurnal variation and its maximum occurs in the nighttime (Lee and Baik 2010). In the nighttime, however, urban

Corresponding author e-mail: Jong-Jin Baik, jjbaik@snu.ac.kr

DOI: 10.1175/JAS-D-16-0276.1

heating–induced circulation/flow is weak because of strong static stability, which suppresses upward motion. Many observational and numerical modeling studies show that the maximum intensity of the UBC is observed in the daytime, more specifically in the late afternoon (Shreffler 1978, 1979; Oliveira et al. 2003; Ryu et al. 2013a; Ganbat et al. 2015a). To reflect this characteristic, theoretical studies that examine a diurnal cycle of the UBC use the heating function that has a maximum in the late afternoon (Ganbat et al. 2015b; Seo et al. 2017).

The general structure of the UBC in the calm atmosphere consists of low-level inward flows toward the urban center, strong updrafts near the urban center, upper-level outward flows, and weak downdrafts outside the urban area. Interestingly, an idealized numerical modeling study indicates that a reversed UBC in which the direction of circulation is opposite to that of the typical UBC is observed in the early morning when the Coriolis force is included, even though the urban area still releases heat (Savijärvi and Liya 2001). Using a numerical model, Ganbat et al. (2015a) confirmed the numerical modeling result of Savijärvi and Liya (2001). Savijärvi and Liya (2001) explained that a reversed UBC (or anti-UBC) is generated as a result of the inertial rotation of the UBC with an inertial period of $12/|\sin\varphi|$ h (where φ is latitude) after surface heat transfer and vertical mixing are calmed down after sunset. However, the basic dynamics of a reversed UBC has not yet been studied, motivating this study.

The purpose of this study is to understand the dynamics of the UBC in a rotating system, particularly the dynamics of a reversed UBC. The governing equations and solutions are provided in section 2. In section 3, the UBC in a rotating system and the dynamics of a reversed UBC are presented and discussed. A summary and conclusions are given in section 4.

2. Governing equations and solutions

To examine the UBC in a rotating system, we consider a two-dimensional, linear, hydrostatic, Boussinesq airflow system with thermal forcing in the zero background wind. Equations that govern perturbations can be written as follows:

$$u_t - fv = -\pi_x - \alpha u, \tag{1}$$

$$v_t + fu = -\alpha v, \tag{2}$$

$$\pi_z = b, \tag{3}$$

$$b_t + N^2 w = \frac{g}{c_p T_0} q - \alpha b, \quad \text{and} \tag{4}$$

$$u_x + w_z = 0, \tag{5}$$

where u, v, and w are the velocities in the x, y, and z directions (zonal, meridional, and vertical velocities), respectively, π is the perturbation kinematic pressure, b is the perturbation buoyancy, f is the Coriolis parameter, α is the coefficient of Rayleigh friction and Newtonian cooling (hereafter, called the frictional coefficient for simplicity), N is the buoyancy frequency, g is the gravitational acceleration, c_p is the specific heat of air at constant pressure, and T_0 is the reference temperature. The thermal forcing q represents the diurnally varying urban heating and is specified to be bell shaped in the horizontal and have an exponential decay in the vertical. The structure of the thermal forcing imitates the resultant spatial temperature pattern over cities:

$$q(x,z,t) = q_0 \frac{a^2}{x^2 + a^2} e^{-z/H} \mathrm{Re}\{e^{i\Omega t}\}, \tag{6}$$

where q_0 is the magnitude of urban heating, a is the half-width of the bell-shaped function, H is the e-folding depth of urban heating, and Ω is the angular frequency of the diurnal variation of urban heating. Note that Eqs. (1)–(5) and the specified urban heating in Eq. (6) are the same as those of Ganbat et al. (2015b), except that the momentum equation in the y direction, the Coriolis force terms, and the zero background wind are considered in the present study.

Equations (1)–(5) can be combined into a single equation for w, which is expressed by

$$[(\partial_t + \alpha)^2 + f^2] w_{zz} + N^2 w_{xx} = \frac{g}{c_p T_0} q_{xx}. \tag{7}$$

Equation (7) is converted to an ordinary differential equation in z by taking the Fourier transform in x ($\rightarrow k$) and t ($\rightarrow \omega$) as follows:

$$\hat{w}_{zz} + N^2 \lambda^2 \hat{w} = \frac{g}{c_p T_0} \lambda^2 \hat{q}, \tag{8}$$

where

$$\lambda^2 = \frac{k^2}{(\omega - i\alpha)^2 - f^2} \quad \text{and} \tag{9a}$$

$$\hat{q}(k,z,\omega) = q_0 a e^{-ak} e^{-z/H} \frac{\delta(\omega - \Omega) + \delta(\omega + \Omega)}{2}. \tag{9b}$$

Here, the Dirac delta function is denoted by δ. The general solution of Eq. (8) is given by

$$\hat{w}(k,z,\omega) = A(k,\omega) e^{iN\lambda z} + B(k,\omega) e^{-iN\lambda z} + \frac{\lambda^2 H^2}{1 + N^2 \lambda^2 H^2} \frac{g}{c_p T_0} \hat{q}, \tag{10}$$

where

$$\lambda(k,\omega)=\begin{cases}\dfrac{k}{(R^2+I^2)^{1/4}}\left[\cos\left(\dfrac{1}{2}\tan^{-1}\dfrac{I}{R}\right)+i\sin\left(\dfrac{1}{2}\tan^{-1}\dfrac{I}{R}\right)\right] & \text{for} \quad R(\omega)\geq 0,\\ \dfrac{k}{(R^2+I^2)^{1/4}}\left[-\sin\left(\dfrac{1}{2}\tan^{-1}\dfrac{I}{R}\right)+i\cos\left(\dfrac{1}{2}\tan^{-1}\dfrac{I}{R}\right)\right] & \text{for} \quad R(\omega)<0,\end{cases} \tag{11a}$$

$$R(\omega)=\omega^2-(\alpha^2+f^2), \quad \text{and} \tag{11b}$$

$$I(\omega)=2\alpha\omega. \tag{11c}$$

Note that the values of α, f, and ω determine the major behaviors of the solution. For $R(\omega) > 0$, the solution mainly exhibits a wavelike behavior in the vertical. On the other hand, for $R(\omega) < 0$, the solution mainly exhibits a decay in the vertical when the possible ranges of sine and cosine terms in $\lambda(k, \omega)$ are considered. In this study, the values of α, f, and ω that make $R(\omega)$ negative will be used to consider cases in which the UBC exhibits very weak wavelike pattern in the vertical. For $R(\omega) < 0$, the real part of λ changes the sign by the sign of $I(\omega)$, whereas the imaginary part of λ is independent of the sign of $I(\omega)$.

Two unknown coefficients $A(k, \omega)$ and $B(k, \omega)$ in Eq. (10) are obtained by applying a flat bottom boundary condition ($\hat{w} = 0$ at $z = 0$) and eliminating the vertically amplifying component [$B(k, \omega) = 0$]. Then, the solution in Fourier-transformed space is expressed by

$$\hat{w}(k,z,\omega)=\frac{C\lambda^2}{1+N^2\lambda^2H^2}e^{-ak}\frac{\delta(\omega-\Omega)+\delta(\omega+\Omega)}{2}\times(e^{-z/H}-e^{i\mathrm{N}\lambda z}), \tag{12}$$

where $C = gq_0aH^2/(c_pT_0)$.

By taking the inverse Fourier transform in k ($\rightarrow x$) and ω ($\rightarrow t$) and choosing the real part, we can obtain the solution of w in physical space:

$$w(x,z,t)=C\int_0^\infty k^2e^{-ak}\cos kx\{e^{-z/H}(X_R\cos\Omega t-X_I\sin\Omega t)-e^{-\gamma z}[X_R\cos(mz+\Omega t)-X_I\sin(mz+\Omega t)]\}\,dk, \tag{13}$$

where

$$X_R=\frac{\Omega^2+N^2H^2k^2-(\alpha^2+f^2)}{[\Omega^2+N^2H^2k^2-(\alpha^2+f^2)]^2+4\alpha^2\Omega^2}, \tag{14a}$$

$$X_I=\frac{2\alpha\Omega}{[\Omega^2+N^2H^2k^2-(\alpha^2+f^2)]^2+4\alpha^2\Omega^2}, \tag{14b}$$

$$m=\mathrm{Re}\{N\lambda(k,\Omega)\}, \quad \text{and} \tag{14c}$$

$$\gamma=\mathrm{Im}\{N\lambda(k,\Omega)\}. \tag{14d}$$

Using Eq. (13) and the Fourier-transformed equations [Eqs. (1)–(5)], we can obtain the solutions of u, v, π, and b. For example, the solutions of u and v are provided as follows:

$$u(x,z,t)=C\int_0^\infty ke^{-ak}\sin kx\{e^{-z/H}(X_R\cos\Omega t-X_I\sin\Omega t)/H-e^{-\gamma z}\langle m[X_R\sin(mz+\Omega t)+X_I\cos(mz+\Omega t)]-\gamma[X_R\cos(mz+\Omega t)-X_I\sin(mz+\Omega t)]\rangle\}\,dk \quad \text{and} \tag{15}$$

$$v(x,z,t)=-Cf\int_0^\infty ke^{-ak}\sin kx\{e^{-z/H}(Y_R\cos\Omega t+Y_I\sin\Omega t)/H+e^{-\gamma z}\langle m[Y_R\cos(mz+\Omega t)-Y_I\sin(mz+\Omega t)]-\gamma[Y_R\sin(mz+\Omega t)+Y_I\cos(mz+\Omega t)]\rangle\}\,dk, \tag{16}$$

where

$$Y_R=\frac{\Omega X_R-\alpha X_I}{\Omega^2+\alpha^2} \quad \text{and} \tag{17a}$$

$$Y_I=\frac{\alpha X_R+\Omega X_I}{\Omega^2+\alpha^2}. \tag{17b}$$

To examine a diurnal cycle of the UBC, the solution of w that corresponds to the urban heating component that is constant with time (w_c; $\Omega_c = 0\,\mathrm{s}^{-1}$) and the solution of w that corresponds to the urban heating component that varies diurnally (w_d; $\Omega_d = 2\pi/24\,\mathrm{h}^{-1}$) are linearly superposed. The magnitudes of urban heating $q_c = 0.2\,\mathrm{J\,kg^{-1}\,s^{-1}}$ and $q_d = 0.19\,\mathrm{J\,kg^{-1}\,s^{-1}}$ are selected for w_c and w_d, respectively. Other parameter values are specified as $N = 0.01\,\mathrm{s}^{-1}$, $T_0 = 283.15\,\mathrm{K}$, $a = 5\,\mathrm{km}$, and $H = 750\,\mathrm{m}$ (Ganbat et al. 2015b). Urban heating is specified to have a maximum at 1700 local time (LT) and a

minimum at 0500 LT by applying $t - 17$ h to time t. Many previous studies that consider the local circulation induced by diurnally varying thermal forcing (sea–land breeze circulation and UBC) have used different frictional coefficients [$(3.2\,\mathrm{h})^{-1}$ in Dalu and Pielke (1989); $(2\,\mathrm{h})^{-1}$ in Ganbat et al. (2015b); $(8.9\,\mathrm{h})^{-1}$ in Li and Chao (2016)]. These studies focused on the circulations in the daytime. This study focuses the evolution of the UBC in the nighttime and early morning with weaker turbulent activity. In this study, $\alpha = 2 \times 10^{-5}\,\mathrm{s}^{-1}$ [$=(13.9\,\mathrm{h})^{-1}$], which is smaller than the frictional coefficient used in the previous studies, is chosen. The integrations in Eqs. (13), (15), and (16) are numerically calculated using the forward scheme with $\Delta k = 2n\pi/10^5\,\mathrm{m}^{-1}$ ($n = 0, 1, 2, \ldots, 10^4$).

3. Results and discussion

a. UBC in a rotating system

Ganbat et al. (2015b) investigated the UBC induced by urban heating in the resting basic-state wind and a nonrotating frame. In Ganbat et al. (2015b), $\alpha = 1/7200\,\mathrm{s}^{-1}$, $q_c = 0.2\,\mathrm{J\,kg^{-1}\,s^{-1}}$, and $q_d = 0.15\,\mathrm{J\,kg^{-1}\,s^{-1}}$ are used. Here, a brief description of their results is given. In the nighttime, the low pressure and the positive buoyancy drive low-level converging flows toward the urban center. Subsequently, updrafts near the urban center, upper-level diverging flows, and then weak downdrafts outside the urban area are induced. This kind of circulation is maintained with diurnal variations in strength and horizontal and vertical scales. The UBC strengthens with time from 0800 LT and attains its maximum intensity in the late afternoon. Although the time of the strongest urban heating is 1700 LT, the strongest horizontal and vertical velocities occur 2 h 2 min and 36 min later than the time of the strongest daytime urban heating, respectively. The time lags between weakest nighttime urban heating and the weakest horizontal and vertical velocities are the same as in the above. Expectably, urban heating induces the typical UBC in terms of circulation direction over an entire day.

Figure 1 shows meridional and vertical velocities, perturbation kinematic pressure, and velocity vector fields (u, w) in the case with the Coriolis force terms. The selected times are 0200, 0600, and 1200 LT, and the Coriolis parameter is evaluated at $\varphi = 30°$N. At 0200 LT, thermally induced zonal converging flows and updrafts in the urban area are evident (Fig. 1a). Generally, the meridional velocity is positive (negative) in the region with negative (positive) zonal velocity, because of the Coriolis effect. At 0600 LT, near-surface zonal diverging flows accompanied with broad and weak downdrafts of approximately 0.3–1-km depth are developed (Fig. 1b), forming a reversed UBC. A reversed

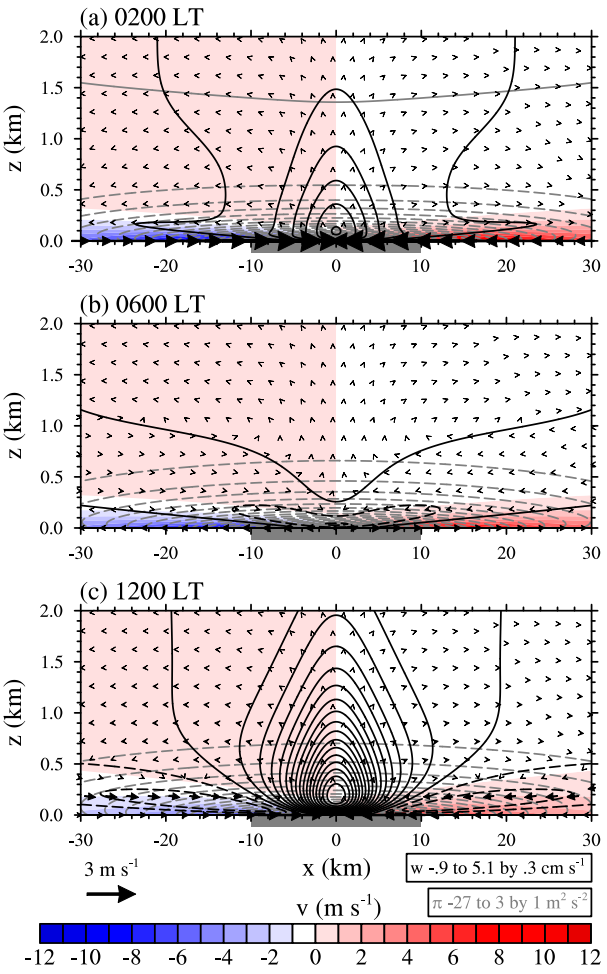

FIG. 1. Meridional (shaded) and vertical (black contours) velocities, perturbation kinematic pressure (gray contours), and velocity vector fields at (a) 0200, (b) 0600, and (c) 1200 LT in the case with the Coriolis force terms. The Coriolis parameter is evaluated at $\varphi = 30°$N. The gray box on the x axis indicates the urban area in which urban heating is concentrated.

UBC is opposite to a typical UBC in terms of circulation direction, even though the kinematic pressure perturbation is negative in the urban area and the thermal forcing is positive (heating). As time goes on, the main updrafts above the downdraft layer strengthen and touch the surface and the circulation direction goes back to that of a typical UBC. At 1200 LT, the typical UBC is well established (Fig. 1c). The zonal converging flows are deeper at 1200 LT than at 0200 LT (Figs. 1a and 1c).

To investigate the latitude dependence of the UBC, we calculate differences in meridional and vertical velocities, perturbation kinematic pressure, and velocity vector between $\varphi = 40°$ and 30°N (the $\varphi = 40°$N case minus the $\varphi = 30°$N case) (Fig. 2). At 0200 (1200) LT, zonal converging near-surface flows are weaker (stronger) in the higher-latitude case. At 0600 LT, the

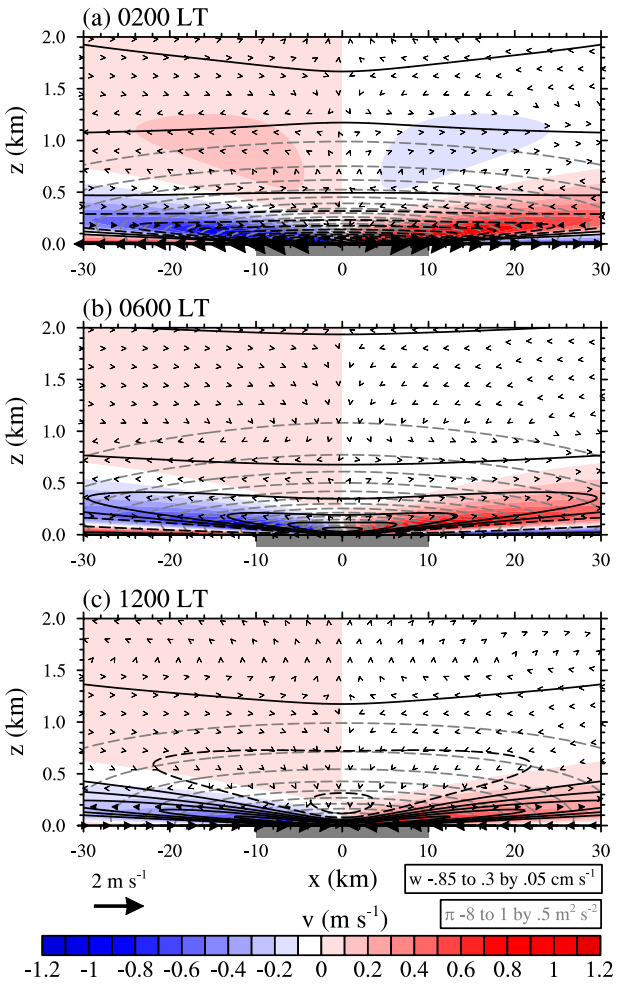

FIG. 2. Fields of differences in meridional (shaded) and vertical (black contours) velocities, perturbation kinematic pressure (gray contours), and velocity vector at (a) 0200, (b) 0600, and (c) 1200 LT between the case of $\varphi = 40°$N and the case of $\varphi = 30°$N.

difference in vertical velocity is positive because weaker low-level downdrafts associated with a reversed UBC are induced in the higher-latitude case. This is related to the fact that the inertial period in the higher latitude is shorter than that in the lower latitude. In section 3b, some discussion of the inertial rotation is provided.

Figure 3 shows differences in meridional and vertical velocities, perturbation kinematic pressure, and velocity vector between the cases with and without the Coriolis force terms (the case with the Coriolis force terms minus the case without the Coriolis force terms). The Coriolis parameter in the case with the Coriolis force terms is evaluated at $\varphi = 30°$N. We use $\alpha = 1/7200\,\mathrm{s}^{-1}$ in these cases because $R(\Omega_d)$ is positive in the case with $\alpha = 2 \times 10^{-5}\,\mathrm{s}^{-1}$ and no Coriolis force. The addition of the Coriolis force terms results in the weakening of zonal converging flows and updrafts during the entire day. Note that in this rotational case with strong friction, a reversed UBC does not appear.

Figure 4 shows the hodographs of the diurnally varying component of surface horizontal velocity at $x = -5$, -10, and -20 km with $\alpha = 2 \times 10^{-5}$ and $1/7200\,\mathrm{s}^{-1}$. The Coriolis parameter is evaluated at $\varphi = 30°$N. The black circle on each trajectory indicates the surface horizontal velocity at 0000 LT, and the spiral curve from the black circle indicates the vertical change of the horizontal velocity at $x = -5$ km and 0000 LT. The surface horizontal velocity rotates clockwise with time, and the horizontal velocity rotates clockwise with height (see the spiral curves in Fig. 4). At $x = -5$ km and 0000 LT, the height from the surface at which the zonal velocity first becomes zero is 20 (40) m in the case with $\alpha = 2 \times 10^{-5}$ ($\alpha = 1/7200$) s^{-1}. In the case with the smaller frictional coefficient (Fig. 4a), the range of diurnal variation in surface zonal velocity is similar to that in surface meridional velocity and the strongest surface horizontal velocity ($6.4\,\mathrm{m\,s}^{-1}$) appears at ~2200 (~1000) LT. The daily constant components of surface horizontal velocity in this case are (4.3, −15.5), (3.2, −11.8), and (1.7, –6.2) $\mathrm{m\,s}^{-1}$ at $x = -5$, -10, and -20 km, respectively. Hence, at these locations, the surface zonal velocity changes sign from 0600 to 1000 LT and the surface meridional velocity does not change sign. Note that the strongest zonal and meridional velocities are $-5.8\,\mathrm{m\,s}^{-1}$ at ~0800 LT and $5.6\,\mathrm{m\,s}^{-1}$ at ~1300 LT, respectively. In the case with the larger frictional coefficient (Fig. 4b), the range of the diurnally varying component is larger in the zonal direction than in the meridional direction and the surface horizontal velocity is the strongest at ~1900 (~0700) LT. The strongest surface horizontal wind speed in this case is $1.9\,\mathrm{m\,s}^{-1}$, which is $4.5\,\mathrm{m\,s}^{-1}$ weaker than that in the case with $\alpha = 2 \times 10^{-5}\,\mathrm{s}^{-1}$. The daily constant components of surface horizontal velocity are (1.9, −1.0), (1.4, −0.7), and (0.7, −0.4) $\mathrm{m\,s}^{-1}$ at $x = -5$, -10, and -20 km, respectively. In this case, the sign of surface zonal and meridional velocities does not change during the entire day. Note that the strongest zonal and meridional velocities are $1.7\,\mathrm{m\,s}^{-1}$ at ~0700 LT and $0.8\,\mathrm{m\,s}^{-1}$ at ~0900 LT, respectively. The horizontal wind speed decreases rapidly with height in both the cases.

b. *Dynamics of reversed UBC*

The occurrence of a reversed UBC is possible if the maximum amplitude of the diurnally varying component of the velocity in the zonal or vertical

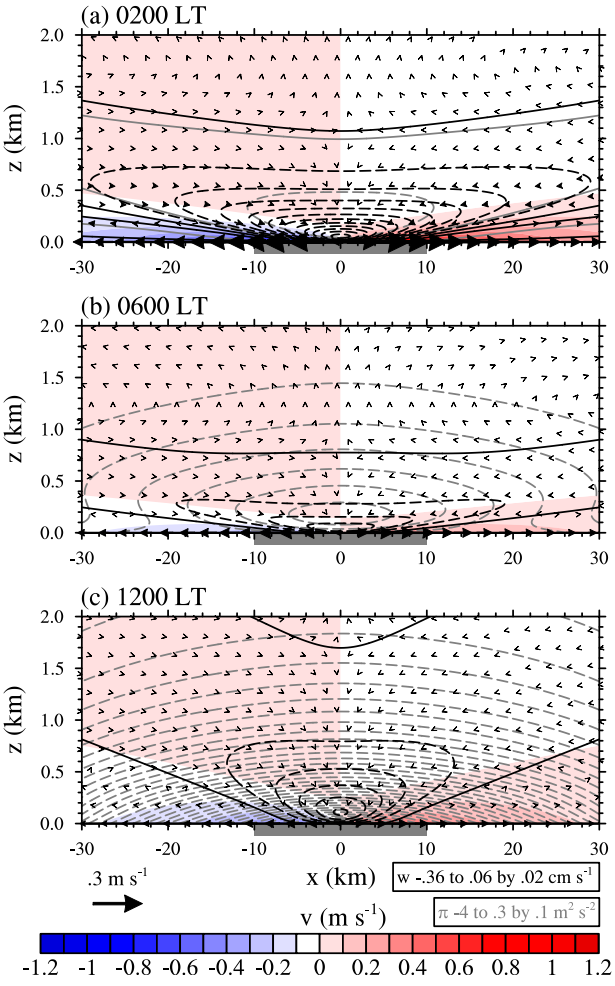

FIG. 3. Fields of differences in meridional (shaded) and vertical (black contours) velocities, perturbation kinematic pressure (gray contours), and velocity vector at (a) 0200, (b) 0600, and (c) 1200 LT between the case with the Coriolis force terms and the case without the Coriolis force terms. The Coriolis parameter in the case with the Coriolis force terms is evaluated at $\varphi = 30°$N.

direction exceeds the value of its daily constant component. To examine the occurrence condition of a reversed UBC, we calculate the maximum value of the diurnally varying vertical velocity ($w_{d,\max}$) for the ranges of the latitude and the frictional coefficient. Also, we calculate the ratio of $w_{d,\max}$ to the daily constant vertical velocity w_c at the occurrence location and time ($t = t_{\max}$) of $w_{d,\max}$. In this analysis, we use $q_c = q_d = 0.2\,\mathrm{J\,kg^{-1}\,s^{-1}}$ to emphasize that the occurrence condition of a reversed UBC is the circulation direction that can be reversed even though the thermal forcing has a positive sign. In the case of $q_d > q_c$, a reversed UBC can appear more easily. Figure 5 shows $w_{d,\max}$, $w_{d,\max}/w_c$, and the occurrence time and height $z_{\max}$ of $w_{d,\max}$. The parameter r is the ratio of the frictional coefficient to the angular frequency of Earth's rotation. The gray area in Fig. 5 indicates the range of $R(\Omega_d) \geq 0$ ($r^2 \leq 1 - 4\sin^2\varphi$). We can regard that a reversed UBC appears at $z = z_{\max}$ after 12 h of $t = t_{\max}$ with the strength $w_{d,\max} - w_c$ because the diurnally varying component has the opposite sign with the same strength after 12 h of $t = t_{\max}$.

The results shown in Fig. 5 are sensitive near $\varphi = 30°$N for small r. The ratio $w_{d,\max}/w_c$ is maximum at $\varphi \sim 30°$N and $r \sim 0$ and generally decreases (increases) with latitude for small (large) r. For a given latitude, the ratio $w_{d,\max}/w_c$ decreases with r except in very low latitudes. Figure 5b indicates that a reversed UBC exists only in high latitudes for a strongly viscous system and that the Coriolis force plays an important role for a weakly viscous system. In the tropics, a reversed UBC does not occur for a strongly viscous system. The Coriolis parameter in λ, X_R, and X_I in Eqs. (11) and (14) acts as a frictional coefficient. In detail, $\alpha^2 + f^2$ is applied in a rotating system in place of α^2 in a nonrotating system such as Eq. (11) in Ganbat et al. (2015b) and Eq. (10) in Seo et al. (2017). Olfe and Lee (1971) also indicated that the Coriolis force damps the heat island–type flows. In the system considered in this study, the zonal pressure gradient produced by urban heating generates zonal flows. In terms of energetics, the Coriolis force diverts part of the driving energy to generate meridional flows, while friction consumes energy on both zonal and meridional flows. In this way, the zonal circulation is weakened by the Coriolis force. For a given r, $w_{d,\max}$ decreases with latitude (Fig. 5a) and $z_{\max}$ increases with latitude (Fig. 5d). For a given latitude, $w_{d,\max}$ also decreases with r (Fig. 5a) and $z_{\max}$ also increases with r (Fig. 5d). The occurrence time of $w_{d,\max}$ for a given latitude higher than ~30°N is delayed with r, but the occurrence time of $w_{d,\max}$ decreases with r for the cases with $t_{\max}$ larger than 30 min in a limited range of latitude and r (Fig. 5c).

The resonance-like pattern of the ratio $w_{d,\max}/w_c$ at $\varphi \sim 30°$N and $r \sim 0$ recalls the work of Rotunno (1983). Rotunno (1983) examined the sea–land breeze represented by an atmospheric response to diurnally varying thermal forcing in the equation system similar to that of this study. Without viscous effects, the generated circulation is confined to the neighborhood of the thermal forcing in the case of $f > \Omega_d$, while the generated circulation is in the form of internal-inertial waves in the case of $f < \Omega_d$. The system is singular at the critical latitude of 30°N. The reversal of the UBC is related to the frictionally decayed resonance of the diurnally varying component of the vertical velocity at $\varphi = 30°$N. This is because at $\varphi = 30°$N, the strength of the diurnally varying

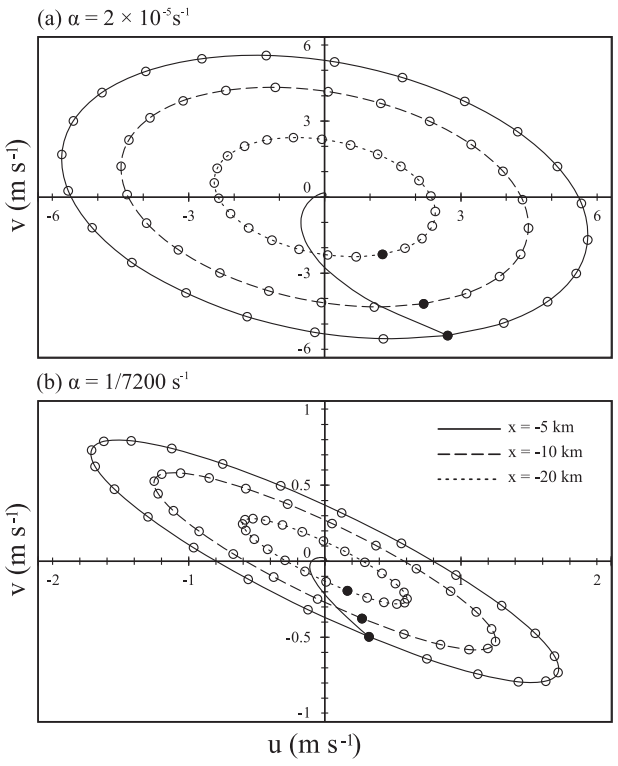

FIG. 4. Hodographs of the diurnally varying component of surface horizontal velocity at $x = -5$, -10, and -20 km and at $\varphi = 30°$N with $\alpha =$ (a) 2×10^{-5} and (b) 1/7200 s^{-1}. The black circle on each trajectory indicates the surface horizontal velocity at 0000 LT, and the spiral curve from the black circle indicates the vertical change of the horizontal velocity at $x = -5$ km and 0000 LT.

component has its maximum, whereas that of the daily constant component of the vertical velocity does not have [Eqs. (13) and (14)].

The solution obtained in this study contains diurnally varying and uniform components because we consider such thermal forcing functions. In a rotating system, thermally induced flow/circulation is always affected by the Coriolis force. By combining Eqs. (1) and (2), we can obtain an equation for the zonal velocity:

$$[(\partial_t + \alpha)^2 + f^2]u = -(\partial_t + \alpha)\pi_x. \tag{18}$$

On the western side of the urban center near the surface, $-\pi_x$ has a positive sign for urban heating. If $-\pi_x$ takes a form of $P_d \cos\Omega(t - t_0) + P_c$, Eq. (18) can be written as

$$[(d_t + \alpha)^2 + f^2]u = \alpha P_d \cos\Omega(t - t_0) - \Omega P_d \sin\Omega(t - t_0) + \alpha P_c. \tag{19}$$

Equation (19) is an oscillation-type equation with the imposed time-dependent forcing. The solutions of u and v are

$$u(t) = \mathrm{Re}\{\tilde{U}_0 e^{(if-\alpha)(t-t_0)}\} + D_d \cos\Omega(t - t_0) + E_d \sin\Omega(t - t_0) + D_c \quad \text{and} \tag{20}$$

$$v(t) = \mathrm{Re}\{i\tilde{U}_0 e^{(if-\alpha)(t-t_0)}\} + F_d \cos\Omega(t - t_0) + G_d \sin\Omega(t - t_0) + F_c, \tag{21}$$

where

$$D_d = \alpha \frac{\Omega^2 + \alpha^2 + f^2}{R^2(\Omega) + I^2(\Omega)} P_d, \tag{22a}$$

$$E_d = \Omega \frac{\Omega^2 + \alpha^2 - f^2}{R^2(\Omega) + I^2(\Omega)} P_d, \tag{22b}$$

$$D_c = -\frac{\alpha}{R(0)} P_c, \tag{22c}$$

$$F_d = f \frac{R(\Omega)}{R^2(\Omega) + I^2(\Omega)} P_d, \tag{22d}$$

$$G_d = -f \frac{I(\Omega)}{R^2(\Omega) + I^2(\Omega)} P_d, \quad \text{and} \tag{22e}$$

$$F_c = \frac{f}{R(0)} P_c. \tag{22f}$$

Here, $\tilde{U}_0$ $(= u_0 + iv_0)$ is the complex velocity at $t = t_0$. Equations (20) and (21) indicate that the solutions of the zonal and meridional velocities induced by a diurnally varying perturbation kinematic pressure gradient have a temporally decaying inertial rotation term, diurnally varying terms, and a constant term. If we consider $t \sim t_0$ as a late afternoon time at which the UBC is strongest, we can estimate the time evolution of horizontal velocity after $t \sim t_0$, which is affected by the Coriolis force and the diurnally varying perturbation kinematic pressure gradient.

The sum of the second and fourth terms in the right-hand sides of Eqs. (20) and (21) has a minimum at $t = t_0 + 12$ h. The minimum value of the sum at $t = t_0 + 12$ h has a sign opposite to the maximum value if $|D_d|$ and $|F_d|$ are larger than $|D_c|$ and $|F_c|$, respectively. The condition for $|D_d| \geq |D_c|$ is $r^2 \leq 12\sin^2\varphi - 1$, and the limit curve is drawn in Fig. 5b. Note that the limit curve is closer to $w_{d,\max}/w_c = 1$ curve for large r. The third terms on the right-hand sides of Eqs. (20) and (21) shift the phase of the times that the maximum and minimum occur. The positive (negative) E_d and G_d indicate that the sum of the second, third, and fourth terms has a minimum value after (before) $t = t_0 + 12$ h. For a given latitude, $t_{\max}$ increases with r in the range of $r^2 \leq 4\sin^2\varphi - 1$ (for $\varphi \geq 30°$N). The limit curve is

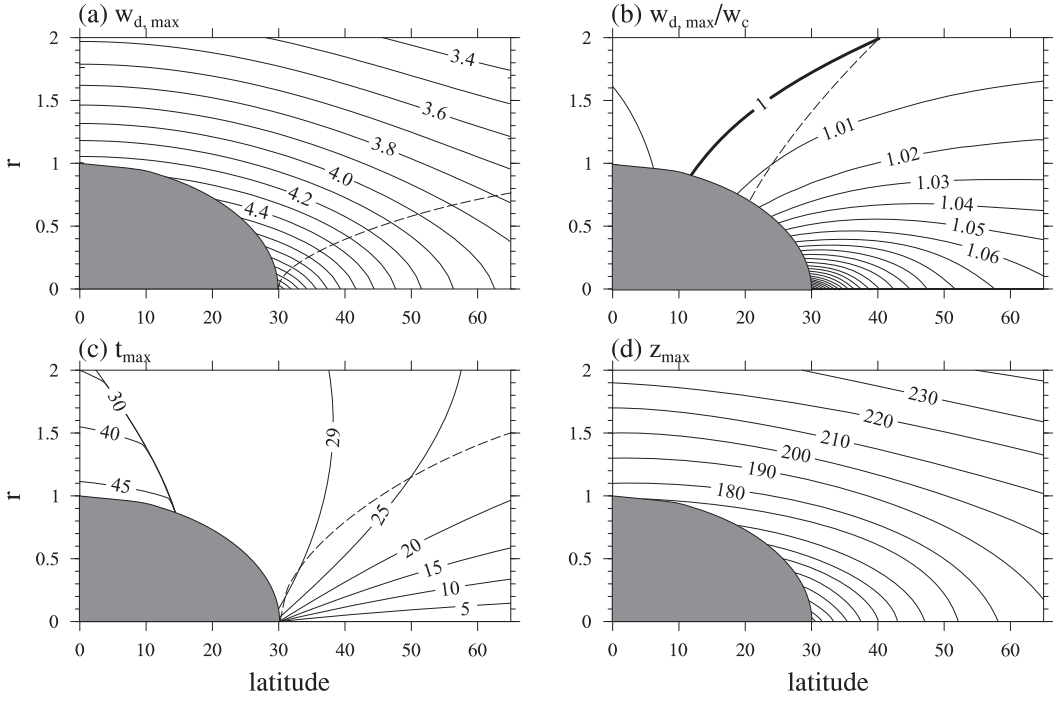

FIG. 5. (a) Maximum diurnally varying vertical velocity (cm s^{-1}), (b) ratio of the maximum diurnally varying vertical velocity to the daily constant vertical velocity, and (c) occurrence time and (d) height (m) of the maximum diurnally varying vertical velocity as a function of latitude and r ($=\alpha/\Omega_d$). Here, we use $q_c = q_d = 0.2\,\mathrm{J\,kg^{-1}\,s^{-1}}$. In (c), the hour of the occurrence time is 17 h and the minute of the occurrence time is contoured. The gray area in which $r^2 \le 1 - 4\sin^2\varphi$ indicates the condition of $R(\Omega_d) \ge 0$. The dashed line in (b) is $r^2 = 12\sin^2\varphi - 1$, and the dashed line in (c) is $r^2 = 4\sin^2\varphi - 1$. For a given φ, the range below the dashed line in (a) indicates $|F_d| \ge |F_c|$ in Eqs. (21) and (22).

drawn in Fig. 5c. Outside of the limit curve, especially for $\varphi < 30°$N, $t_{\max}$ tends to decrease with r for a given latitude. Similarly, we can obtain the condition for $|F_d| \ge |F_c|$ (the limit curve is drawn in Fig. 5a). However, as discussed earlier, there is no sign change of meridional velocity at a given location under all conditions. This is because we consider $v_c \propto -(u_c\sin\varphi)/r$ and $v_d \propto -(ru_d\sin\varphi)/(1 + r^2)$ in the equation system. Note that these relations can be obtained by applying 0, $i\Omega_d v_d$, $2\Omega_d\sin\varphi$, and $r\Omega_d$ to $\partial_t v_c$, $\partial_t v_d$, f, and α in Eq. (2), respectively. The relations indicate that v_c has a larger value than v_d with comparable u_c and u_d for a given latitude.

The complex velocity $\tilde{U}_0$ in the first terms on the right-hand sides of Eqs. (20) and (21) inertially rotates 180° during half an inertial period (12/|sinφ| h). Therefore, for a given r, the minimum of the resultant zonal velocity occurs earlier than the time that is determined by the last three terms on the right-hand sides of Eqs. (20) and (21) in higher latitude. This effect is stronger for smaller r.

Figure 6 shows the time series of $u(t + t_0)$ in Eq. (20) with $r = 0.5$ and 1.5. Here, $(u_0, v_0) = (5, 0)\,\mathrm{m\,s^{-1}}$ and $P_c = P_d = 2.5 \times 10^{-4}\,\mathrm{m\,s^{-2}}$ are used. For $r = 0.5$, the minimum value of the diurnally varying u, which is marked by circles, occurs later (earlier) than $t = t_0 + 12$ h at $\varphi = 40°$N (30°N) following the sign of E_d. Note that the sign of E_d is negative at $\varphi = 40°$N and positive at $\varphi = 30°$N. Moreover, shorter inertial period at $\varphi = 40°$N causes the minimum of total u to occur earlier. From Fig. 6a, we can deduce that the strongest reversed UBC appears earlier and is weaker at $\varphi = 40°$N than at $\varphi = 30°$N. This explains the positive difference in the vertical velocity in Fig. 2b. For $r = 1.5$, negative E_d appears only in $\varphi \ge 64.3°$N and the inertial rotation term is strongly dampened in the nighttime (Fig. 6b). For this reason, it is difficult for a reversed UBC to occur in the strongly viscous system.

4. Summary and conclusions

To examine the dynamics of the urban breeze circulation (UBC) in a rotating system, particularly of a reversed UBC, we constructed a linearized, two-dimensional, hydrostatic, Boussinesq airflow system in the calm atmosphere with specified thermal forcing that represents diurnally varying urban heating. To

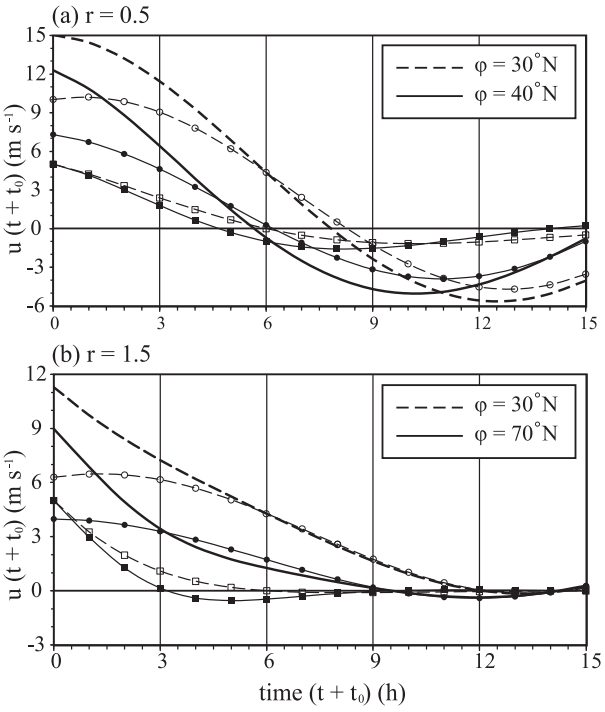

FIG. 6. Time series of $u(t + t_0)$ in Eq. (20) with (a) $r = 0.5$ at $\varphi = 30°$ and 40°N and (b) $r = 1.5$ at $\varphi = 30°$ and 70°N. The first term (inertial rotation) is marked by squares and the sum of the other three terms (diurnal variation) is marked by circles. The thick solid and dashed lines without marks are total $u(t + t_0)$.

represent a diurnal variation of the UBC, a daily steady solution and a diurnally varying solution are linearly superposed.

It was confirmed that the reversed UBC appears in the early morning. Similar to the frictional coefficient, the Coriolis parameter plays a role in damping the strength of the UBC. The occurrence condition, strength, and vertical structure of a reversed UBC were examined. The Coriolis force as well as urban heating alters the occurrence time of a reversed UBC. For a strongly viscous system, a reversed UBC occurs only in high latitudes with low occurrence possibility. An analysis of the solutions for a simple oscillation-type model also shows that the Coriolis force alters the occurrence time and strength of a reversed UBC.

Observational evidence of a reversed UBC is not reported yet. The detection of a reversed UBC might not be straightforward because various kinds of atmospheric flows/circulations interact nonlinearly depending on the geographical location and real urban areas are very complex. Nevertheless, the detection of a reversed UBC in the early morning could be possible if synoptic and other mesoscale flows are very weak. In the presence of a reversed UBC, near-surface thermal structure and pollutant dispersion could be modified. A reversed UBC is expected to be observed.

In this study, we considered constant static stability to simplify the mathematical problem. In the real atmosphere, however, static stability varies diurnally and diurnally varying static stability can significantly affect the strength and vertical structure of the UBC. The dynamics of a UBC or a reversed UBC with diurnally varying static stability deserves an investigation. In this study, we considered a two-dimensional dynamical frame. In three dimensions, the horizontal structure of urban heating can be represented by a circular or elliptic shape, thus closely imitating real urban heating. An extension to three dimensions for the study of the dynamics of a UBC or a reversed UBC would be an interesting research topic.

Acknowledgments. The authors are grateful to three anonymous reviewers for providing valuable comments on this work. This work was funded by the Korea Meteorological Administration Research and Development Program under Grant KMIPA2015-5100 and also by the Mid-career Research Program through a National Research Foundation (NRF) grant funded by the Ministry of Science, ITC and Future Planning (MSIP) (2016R1A2B2013549).

REFERENCES

Baik, J.-J., 1992: Response of a stably stratified atmosphere to low-level heating—An application to the heat island problem. *J. Appl. Meteor.*, **31**, 291–303, doi:10.1175/1520-0450(1992)031<0291:ROASSA>2.0.CO;2.

Barlag, A.-B., and W. Kuttler, 1990: The significance of country breezes for urban planning. *Energy Build.*, **15**, 291–297, doi:10.1016/0378-7788(90)90001-Y.

Clarke, J. F., 1969: Nocturnal urban boundary layer over Cincinnati, Ohio. *Mon. Wea. Rev.*, **97**, 582–589, doi:10.1175/1520-0493(1969)097<0582:NUBLOC>2.3.CO;2.

Dalu, G. A., and R. A. Pielke, 1989: An analytical study of the sea breeze. *J. Atmos. Sci.*, **46**, 1815–1825, doi:10.1175/1520-0469(1989)046<1815:AASOTS>2.0.CO;2.

Dandou, A., M. Tombrou, and N. Soulakellis, 2009: The influence of the city of Athens on the evolution of the sea-breeze front. *Bound.-Layer Meteor.*, **131**, 35–51, doi:10.1007/s10546-008-9306-x.

Draxler, R. R., 1986: Simulated and observed influence of the nocturnal urban heat island on the local wind field. *J. Climate Appl. Meteor.*, **25**, 1125–1133, doi:10.1175/1520-0450(1986)025<1125:SAOIOT>2.0.CO;2.

Estoque, M. A., and C. M. Bhumralkar, 1969: Flow over a localized heat source. *Mon. Wea. Rev.*, **97**, 850–859, doi:10.1175/1520-0493(1969)097<0850:FOALHS>2.3.CO;2.

Ganbat, G., J.-J. Baik, and Y.-H. Ryu, 2015a: A numerical study of the interactions of urban breeze circulation with mountain

slope winds. *Theor. Appl. Climatol.*, **120**, 123–135, doi:10.1007/s00704-014-1162-7.

——, J. M. Seo, J.-Y. Han, and J.-J. Baik, 2015b: A theoretical study of the interactions of urban breeze circulation with mountain slope winds. *Theor. Appl. Climatol.*, **121**, 545–555, doi:10.1007/s00704-014-1252-6.

Haeger-Eugensson, M., and B. Holmer, 1999: Advection caused by the urban heat island circulation as a regulating factor on the nocturnal urban heat island. *Int. J. Climatol.*, **19**, 975–988, doi:10.1002/(SICI)1097-0088(199907)19:9<975::AID-JOC399>3.0.CO;2-J.

Han, J.-Y., and J.-J. Baik, 2008: A theoretical and numerical study of urban heat island–induced circulation and convection. *J. Atmos. Sci.*, **65**, 1859–1877, doi:10.1175/2007JAS2326.1.

Lee, S.-H., and J.-J. Baik, 2010: Statistical and dynamical characteristics of the urban heat island intensity in Seoul. *Theor. Appl. Climatol.*, **100**, 227–237, doi:10.1007/s00704-009-0247-1.

Lemonsu, A., and V. Masson, 2002: Simulation of a summer urban breeze over Paris. *Bound.-Layer Meteor.*, **104**, 463–490, doi:10.1023/A:1016509614936.

Li, Y., and J. Chao, 2016: An analytical solution for three-dimensional sea–land breeze. *J. Atmos. Sci.*, **73**, 41–54, doi:10.1175/JAS-D-14-0329.1.

Lin, Y.-L., and R. B. Smith, 1986: Transient dynamics of airflow near a local heat source. *J. Atmos. Sci.*, **43**, 40–49, doi:10.1175/1520-0469(1986)043<0040:TDOANA>2.0.CO;2.

Lindén, J., and B. Holmer, 2011: Thermally induced wind patterns in the Sahelian city of Ouagadougou, Burkina Faso. *Theor. Appl. Climatol.*, **105**, 229–241, doi:10.1007/s00704-010-0383-7.

Oke, T. R., 1973: City size and the urban heat island. *Atmos. Environ.*, **7**, 769–779, doi:10.1016/0004-6981(73)90140-6.

Olfe, D. B., and R. L. Lee, 1971: Linearized calculations of urban heat island convection effects. *J. Atmos. Sci.*, **28**, 1374–1388, doi:10.1175/1520-0469(1971)028<1374:LCOUHI>2.0.CO;2.

Oliveira, A., R. D. Bornstein, and J. Soares, 2003: Annual and diurnal wind patterns in the city of São Paulo. *Water, Air, Soil Pollut.: Focus*, **3**, 3–15, doi:10.1023/A:1026090103764.

Rotunno, R., 1983: On the linear theory of the land and sea breeze. *J. Atmos. Sci.*, **40**, 1999–2009, doi:10.1175/1520-0469(1983)040<1999:OTLTOT>2.0.CO;2.

Ryu, Y.-H., and J.-J. Baik, 2013: Daytime local circulations and their interactions in the Seoul metropolitan area. *J. Appl. Meteor. Climatol.*, **52**, 784–801, doi:10.1175/JAMC-D-12-0157.1.

——, ——, and J.-Y. Han, 2013a: Daytime urban breeze circulation and its interaction with convective cells. *Quart. J. Roy. Meteor. Soc.*, **139**, 401–413, doi:10.1002/qj.1973.

——, ——, K.-H. Kwak, and N. Moon, 2013b: Impacts of urban land-surface forcing on ozone air quality in the Seoul metropolitan area. *Atmos. Chem. Phys.*, **13**, 2177–2194, doi:10.5194/acp-13-2177-2013.

Savijärvi, H., and J. Liya, 2001: Local winds in a valley city. *Bound.-Layer Meteor.*, **100**, 301–319, doi:10.1023/A:1019215031007.

Seo, J. M., G. Ganbat, J.-Y. Han, and J.-J. Baik, 2017: Theoretical calculations of interactions between urban breezes and mountain slope winds in the presence of basic-state wind. *Theor. Appl. Climatol.*, **127**, 865–874, doi:10.1007/s00704-015-1674-9.

Shreffler, J. H., 1978: Detection of centripetal heat island circulations from tower data in St. Louis. *Bound.-Layer Meteor.*, **15**, 229–242, doi:10.1007/BF00121924.

——, 1979: Heat island convergence in St. Louis during calm periods. *J. Appl. Meteor.*, **18**, 1512–1520, doi:10.1175/1520-0450(1979)018<1512:HICISL>2.0.CO;2.